Supplementary Information

The first exploration of coordination chemistry using a methyl substituted *o*-vanillin based ligand: Example started with Dy_4/Zn_2Dy_2 systems displaying slow relaxation of magnetization

Anangamohan Panja*[a,b] Zvonko Jagličić,[c] Radovan Herchel,[d] Paula Brandão,[e] Kuheli Pramanik [a,b] and Narayan Ch. Jana,[a]

[a] *Department of Chemistry, Panskura Banamali College, Panskura RS, WB 721152, India*

[b] *Department of Chemistry, Gokhale Memorial Girls' College, 1/1 Harish Mukherjee Road, Kolkata-700020, India.*

[c] *Institute of Mathematics, Physics and Mechanics & Faculty of Civil and Geodetic Engineering, University of Ljubljana, Jadranska 19, 1000 Ljubljana, Slovenia*

[d] *Department of Inorganic Chemistry, Faculty of Science, Palacký University, 17. listopadu 12, 77146 Olomouc, Czech Republic*

[e] *Department of Chemistry, CICECO-Aveiro Institute of Materials, University of Aveiro, 3810-193 Aveiro, Portugal*

* Corresponding author e-mail: ampanja@yahoo.co.in

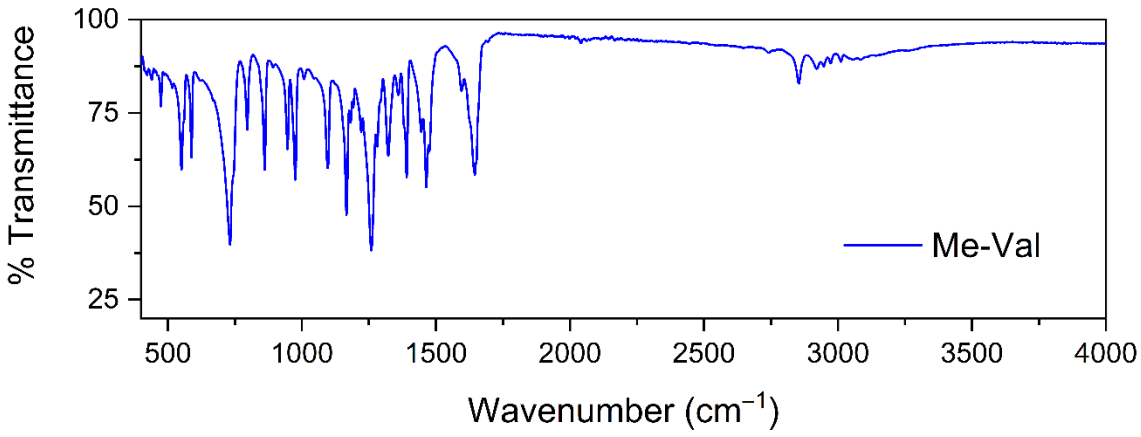

Fig. S1: FTIR spectrum of 2-hydroxy-3-methoxy-5-methylbenzaldehyde. (Me-val).

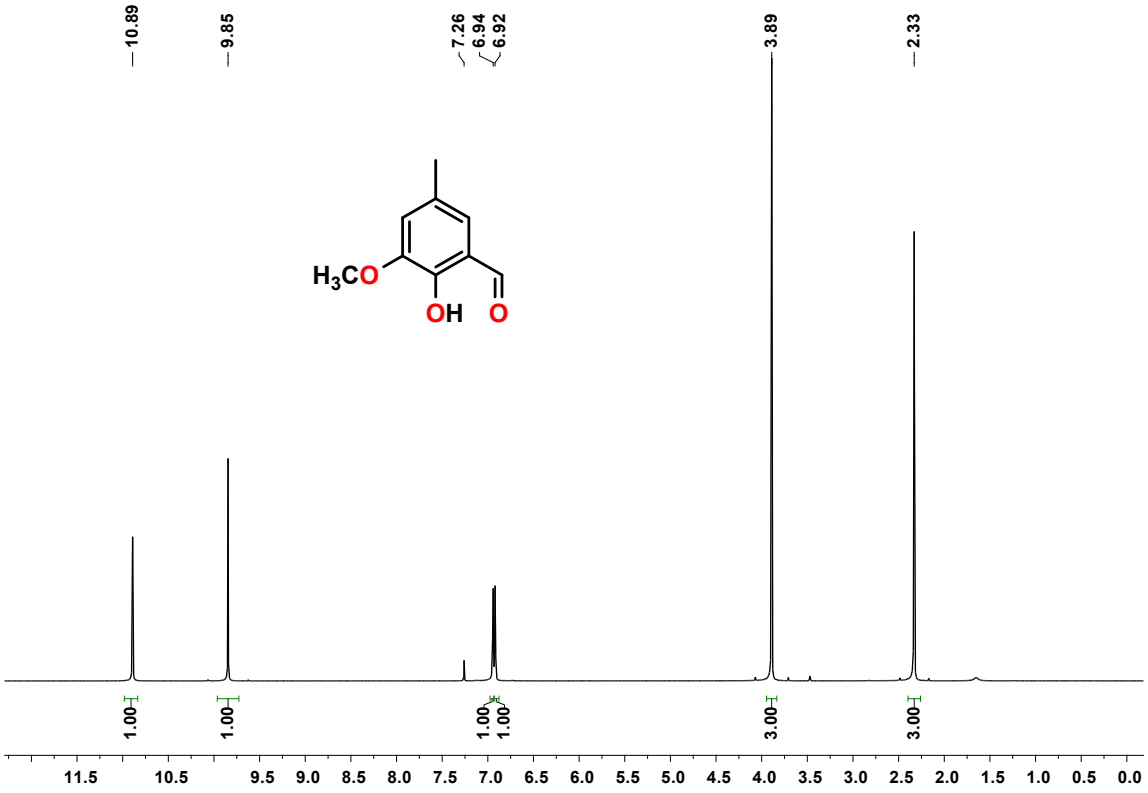

Fig. S2. ^{1}H NMR of 2-hydroxy-3-methoxy-5-methylbenzaldehyde in $CDCl_3$ at r.t.

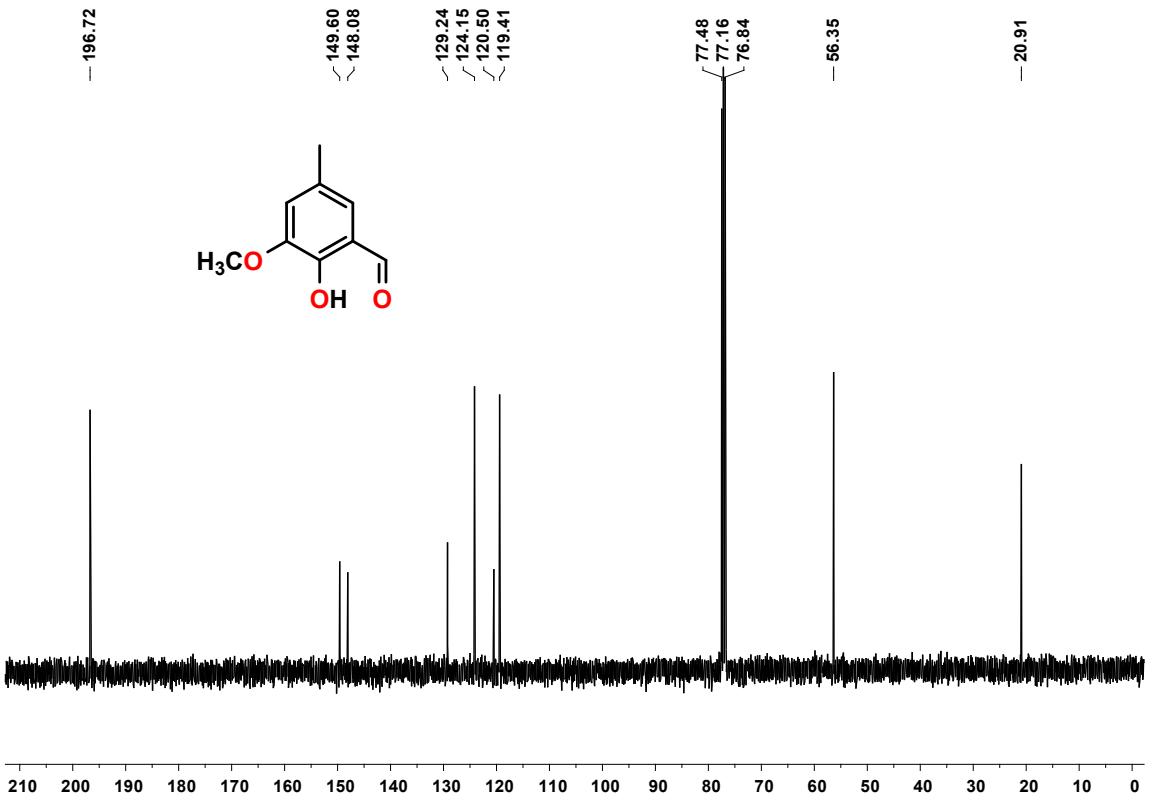

Fig. S3: ^{13}C NMR of 2-hydroxy-3-methoxy-5-methylbenzaldehyde in $CDCl_3$ at r.t.

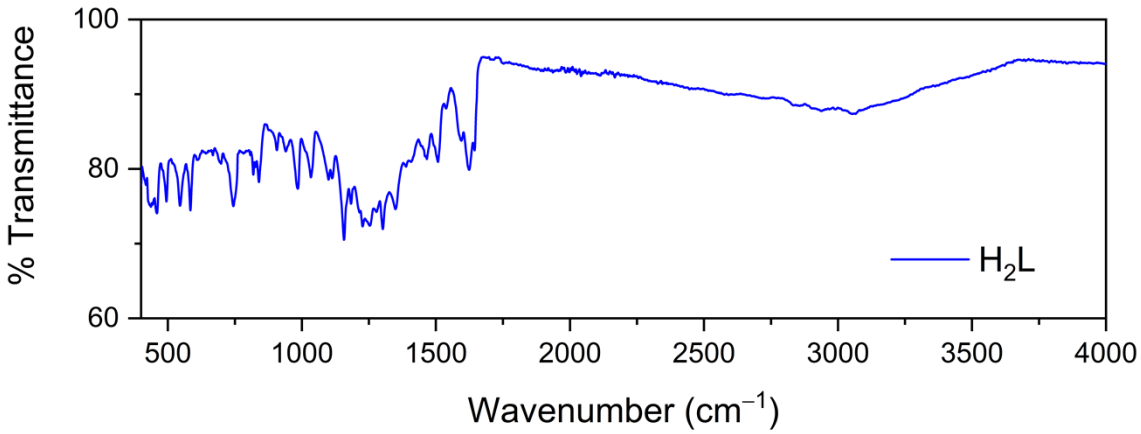

Fig. S4: FTIR spectrum of Schiff base ligand (E)-2-[(2-hydroxyphenyl)iminomethyl]-6-methoxy-4-methylphenol (H_2L).

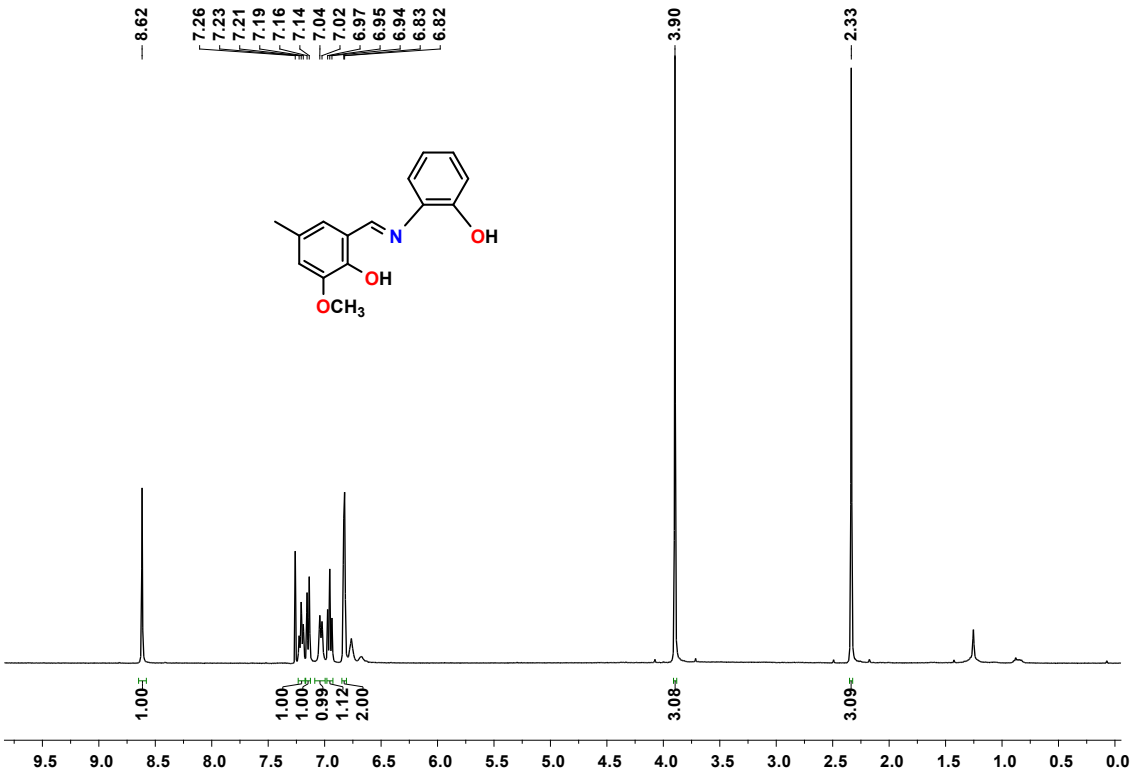

Fig. S5. ^{1}H NMR of Schiff base ligand (E)-2-[(2-hydroxyphenyl)iminomethyl]-6-methoxy-4-methylphenol (**H_2L**) in $CDCl_3$ at r.t.

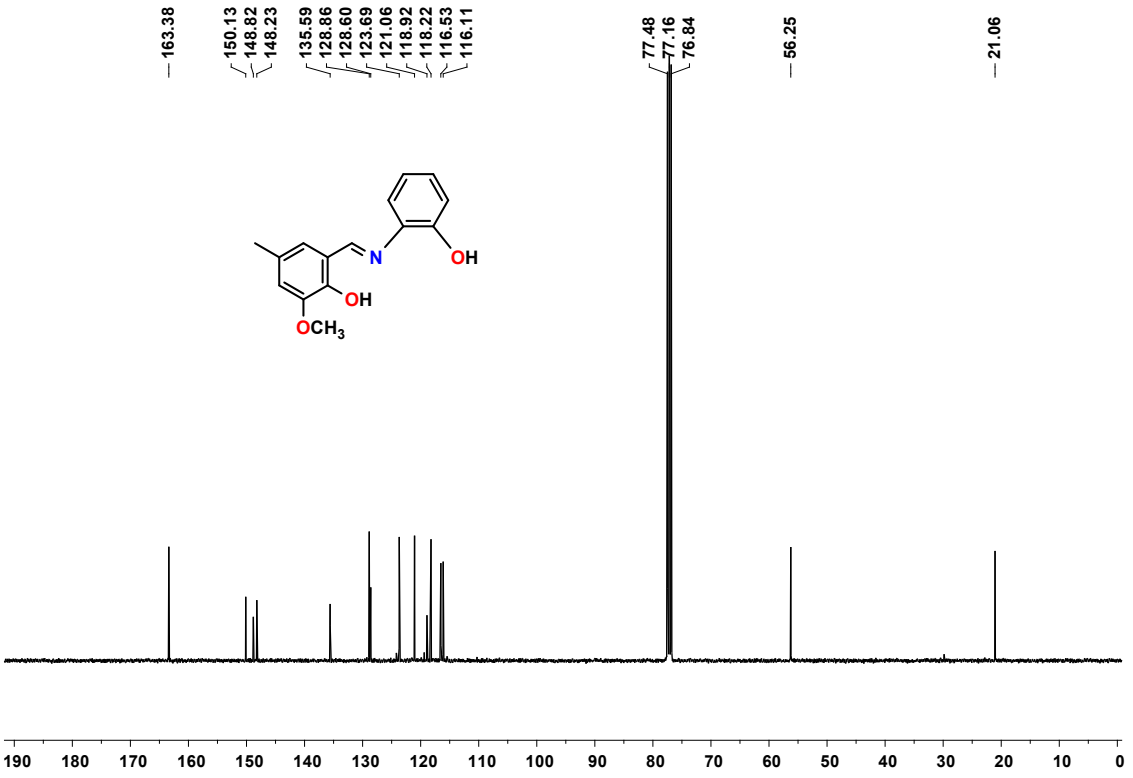

Fig. S6: ^{13}C NMR of Schiff base ligand (E)-2-[(2-hydroxyphenyl)iminomethyl]-6-methoxy-4-methylphenol (**H_2L**) in $CDCl_3$ at r.t.

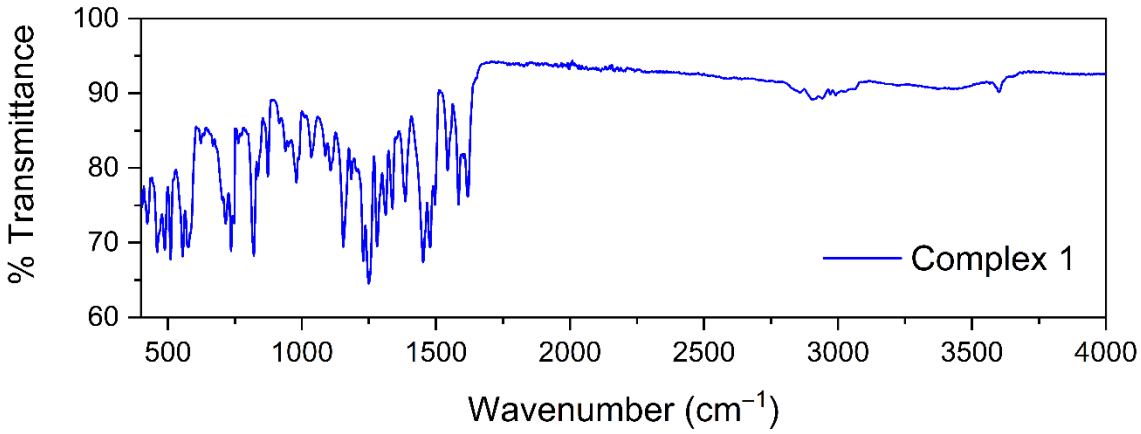

Fig. S7: FTIR spectrum of complex **1**.

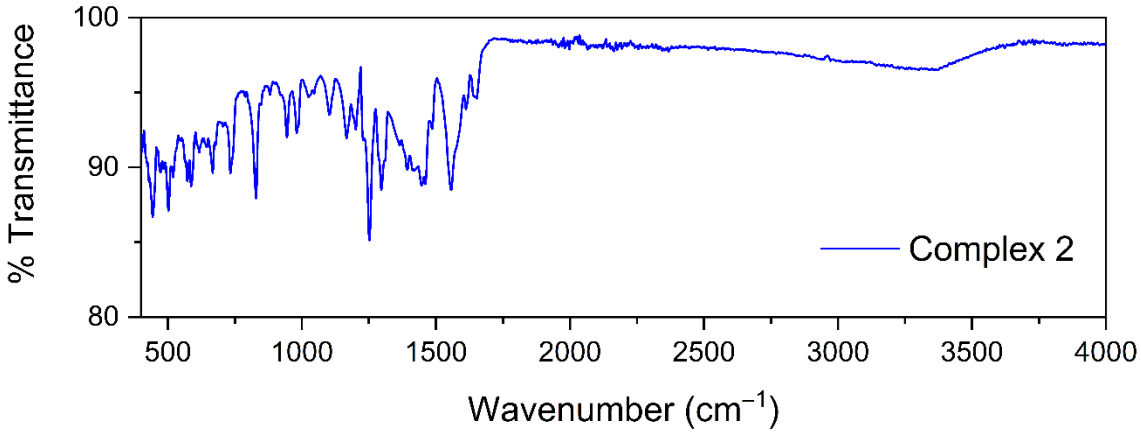

Fig. S8: FTIR spectrum of complex **2**.

(a)

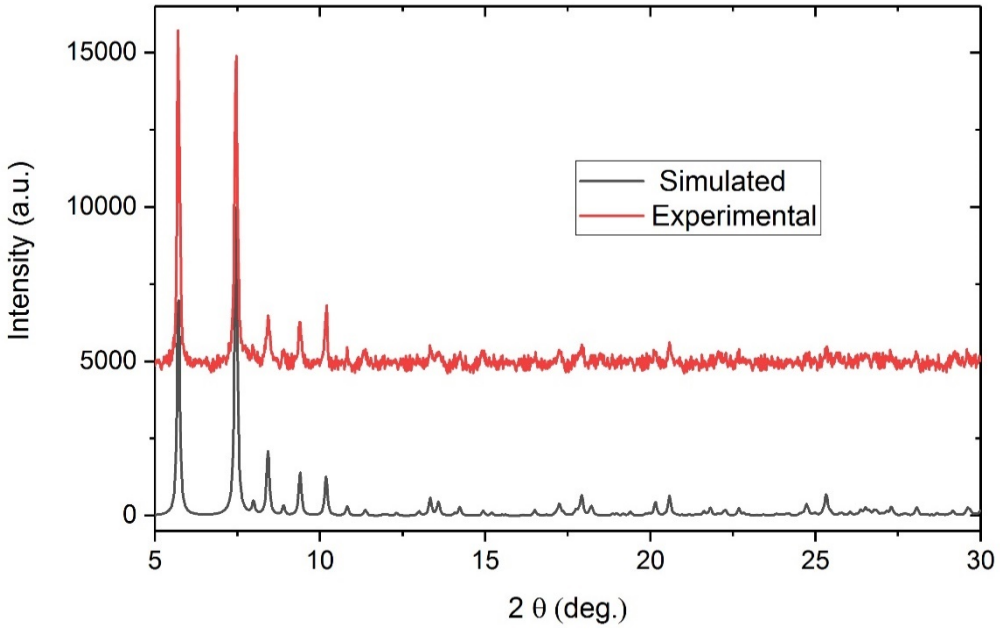

(b)

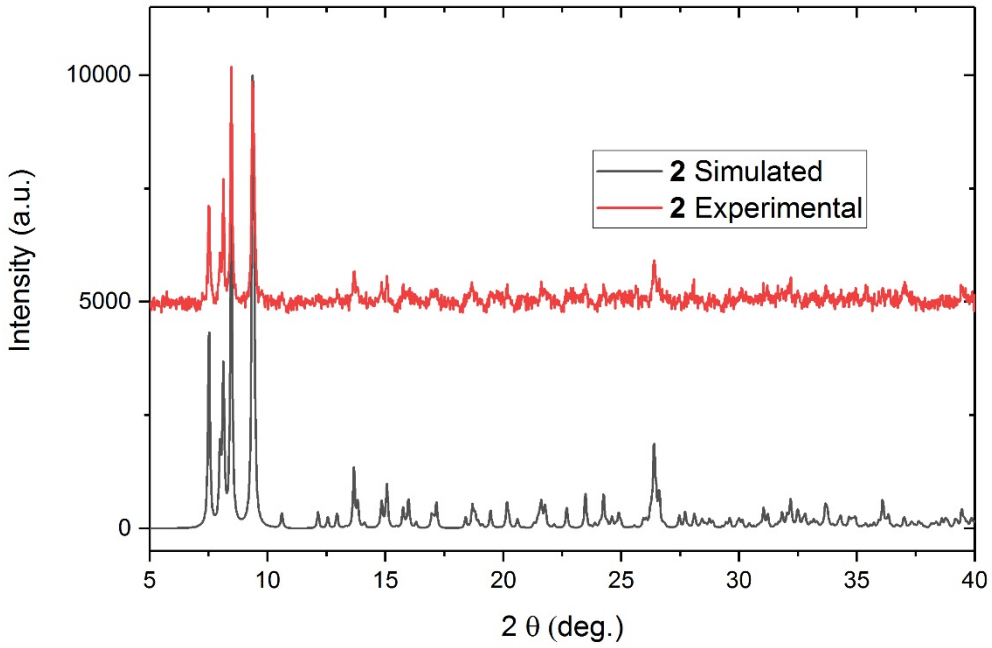

Fig. S9: (a) and (b) represent experimental and simulated PXRD patterns of **1** and **2**.

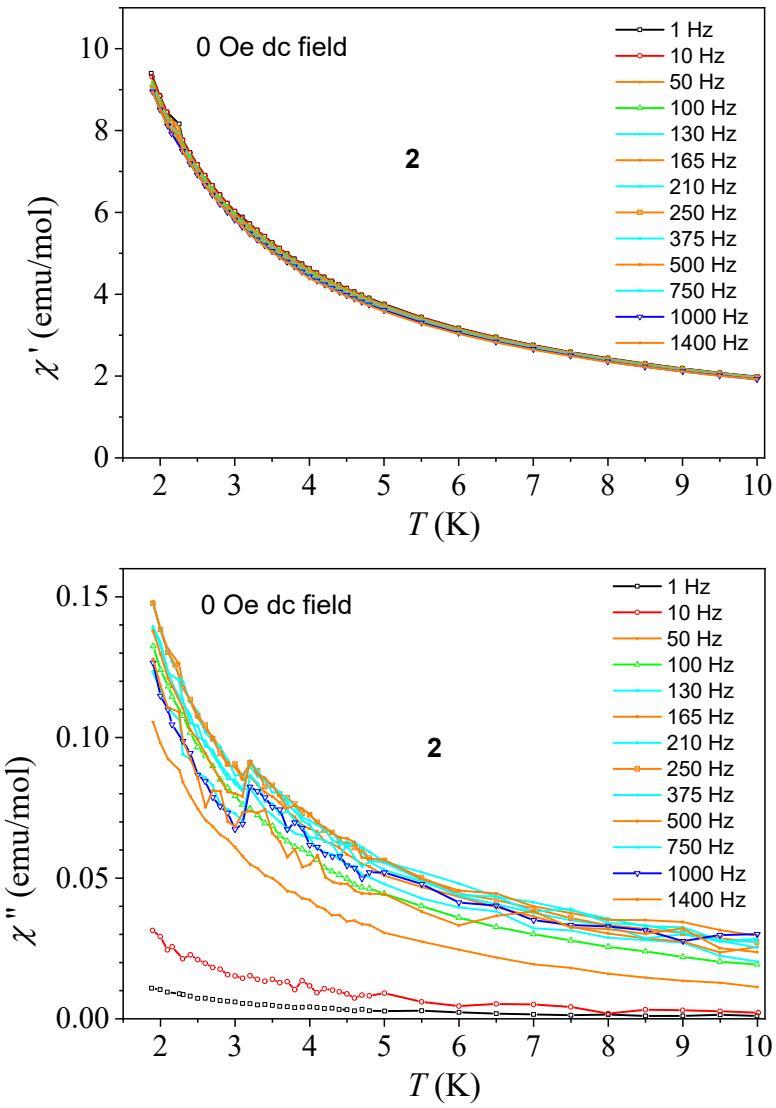

Fig. S10. AC susceptibility of complex **2** measured in 0 Oe dc magnetic field. The amplitude of the ac magnetic field is 6 Oe.

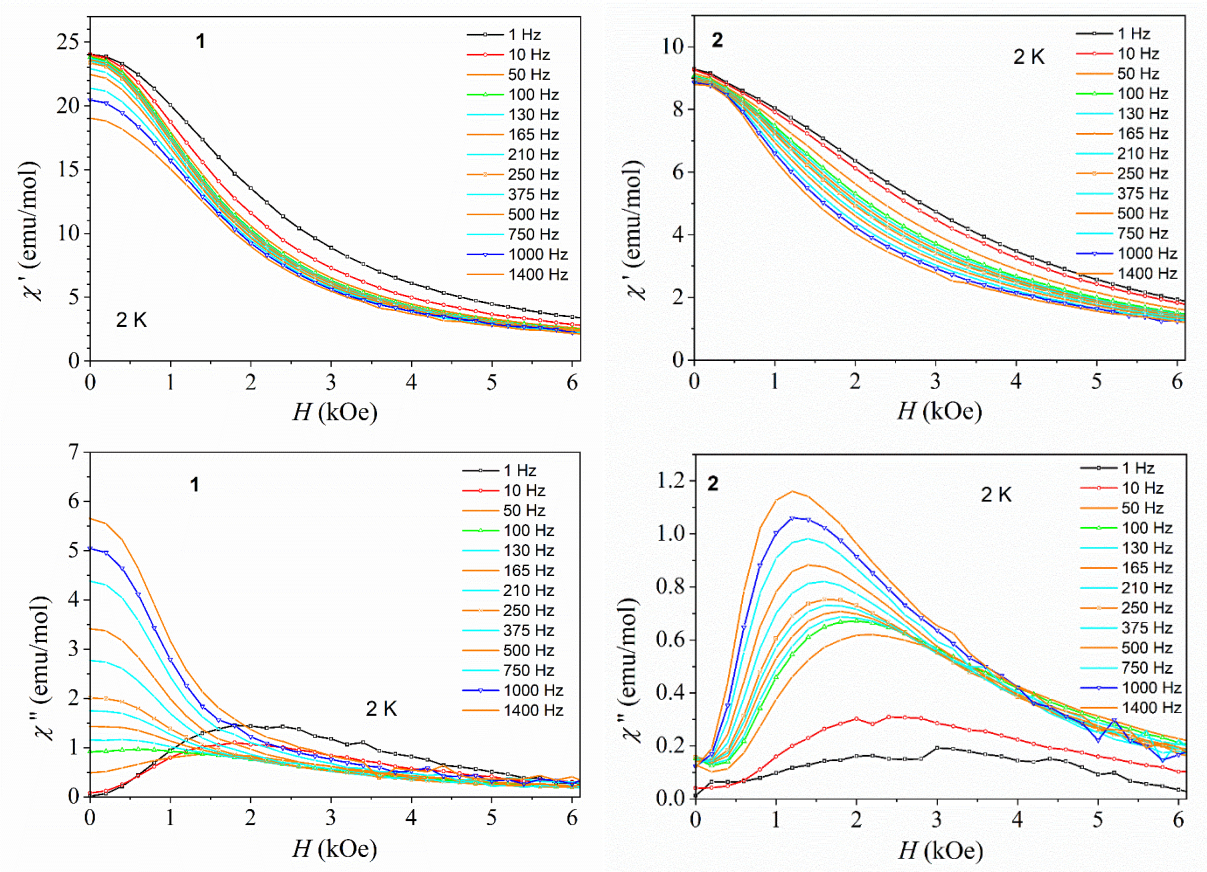

Fig. S11. Temperature-dependence of in-phase and out-of-phase AC susceptibilities of **1** (left) and **2** (right) measured at 2 K for different dc magnetic fields. The amplitude of the ac magnetic field is 6 Oe.

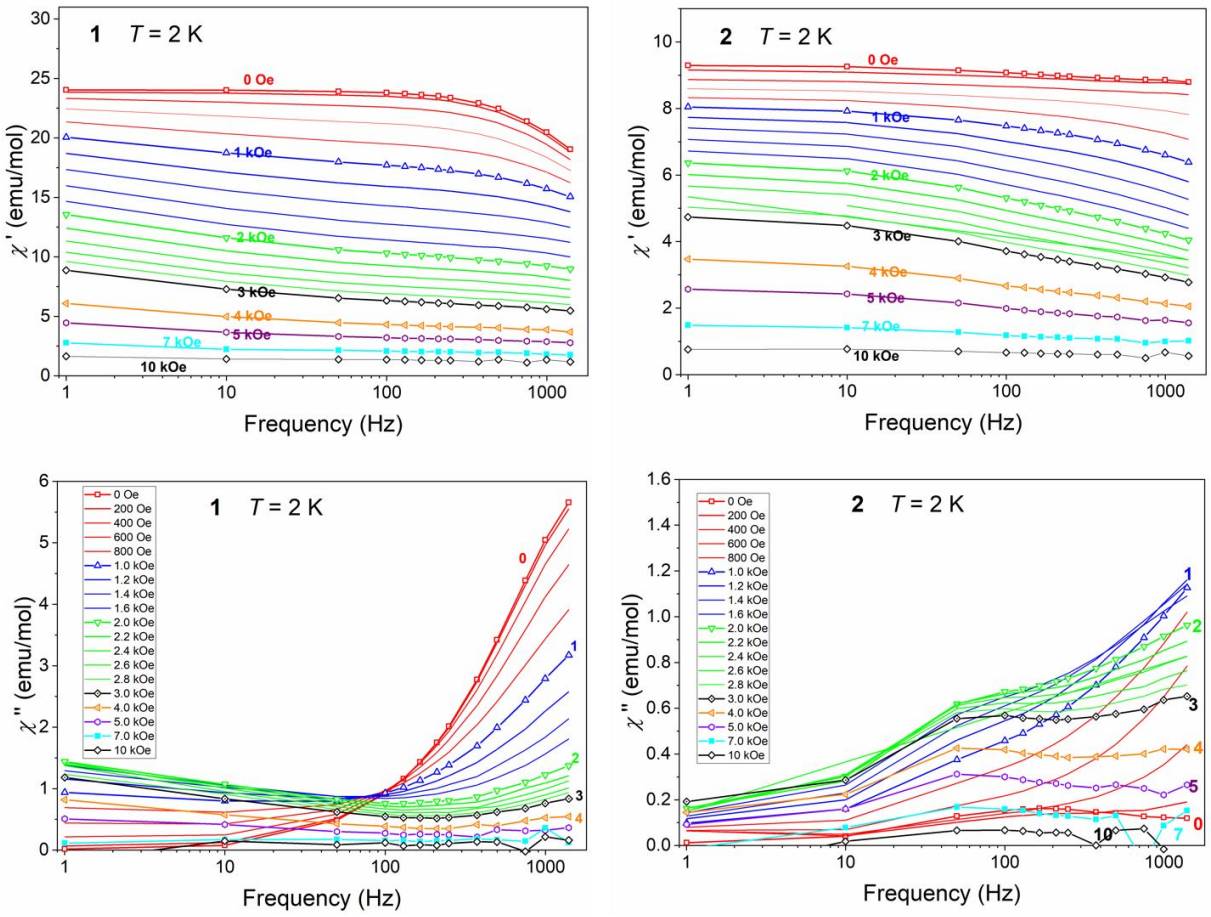

Fig. S12. Frequency-dependence of in-phase and out-of-phase AC susceptibilities of **1** (left) and **2** (right) measured at 2 K for different dc magnetic fields. The amplitude of the ac magnetic field is 6 Oe.

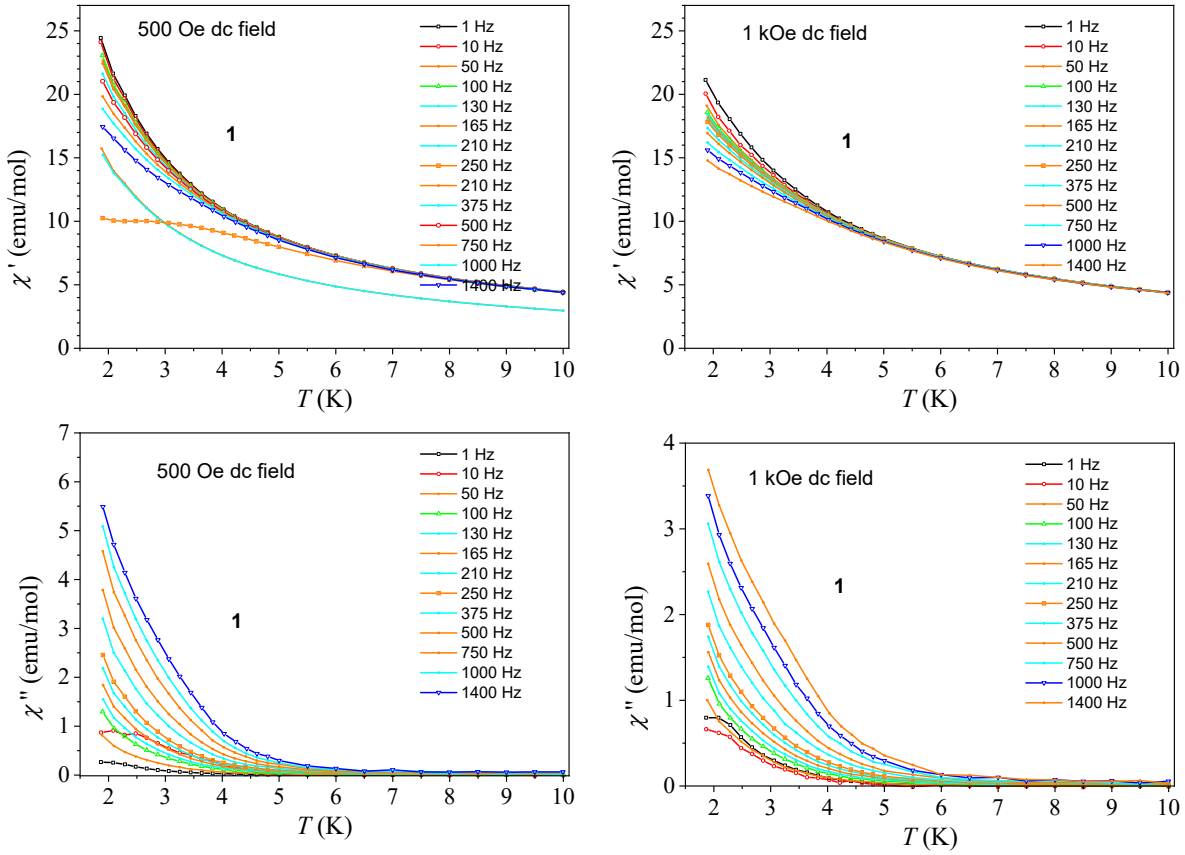

Fig. S13. AC susceptibility of complex **1** measured in 500 Oe dc magnetic field (left) and 1000 Oe dc magnetic field (right). The amplitude of the ac magnetic field is 6 Oe.

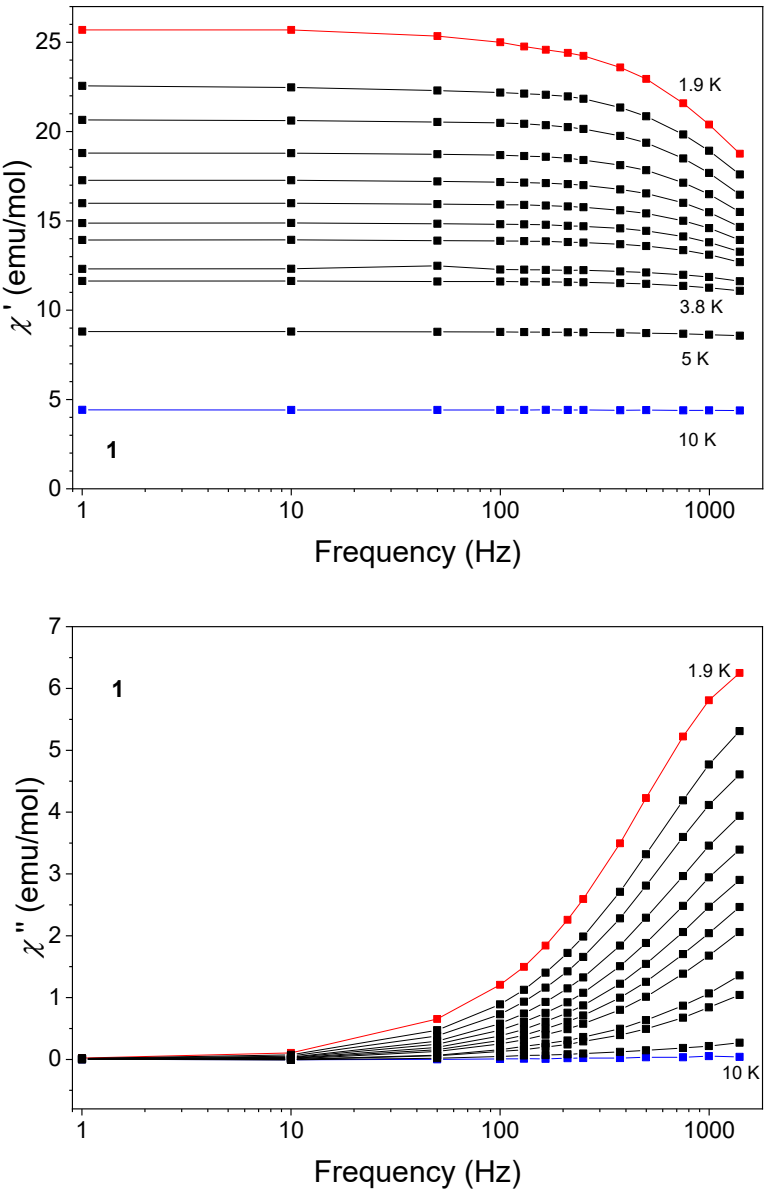

Fig. S14. AC susceptibility of complex **1** measured in 0 Oe dc magnetic field as a function of the frequency of applied magnetic field. The amplitude of the ac magnetic field is 6 Oe.

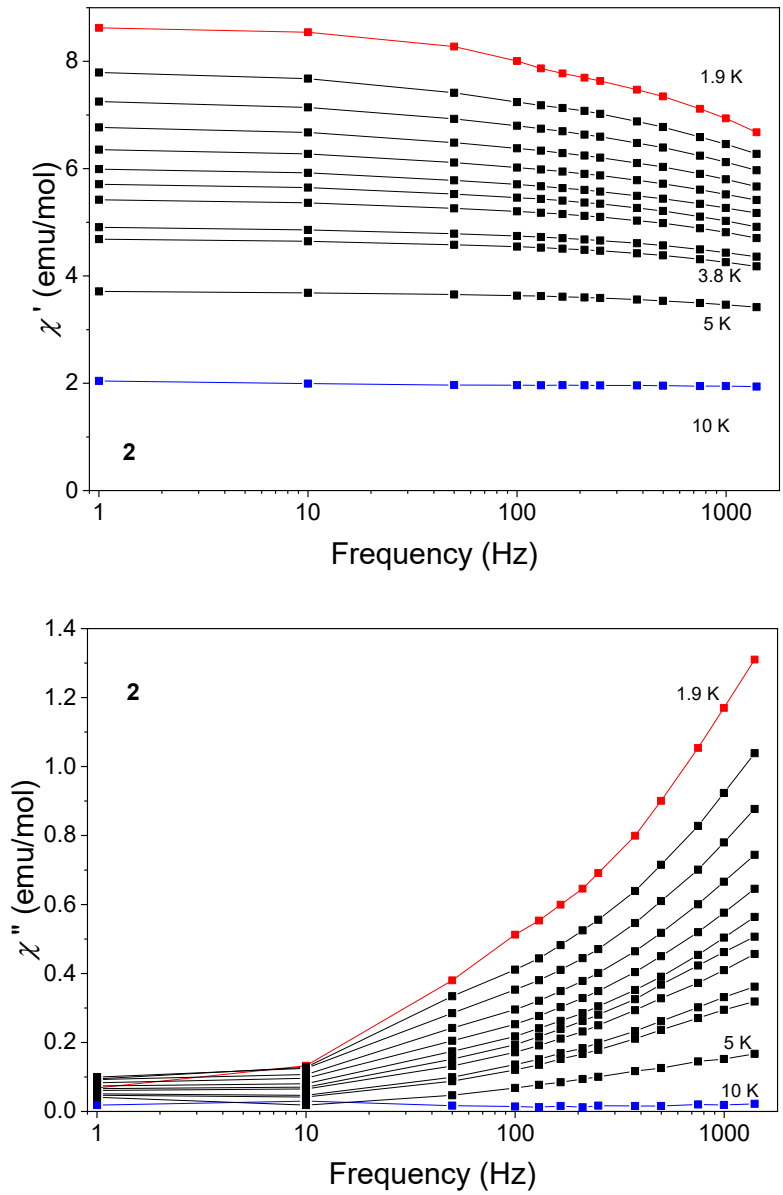

Fig. S15 AC susceptibility of complex **2** measured in 1000 Oe dc magnetic field as a function of the frequency of applied magnetic field. The amplitude of the ac magnetic field is 6 Oe.

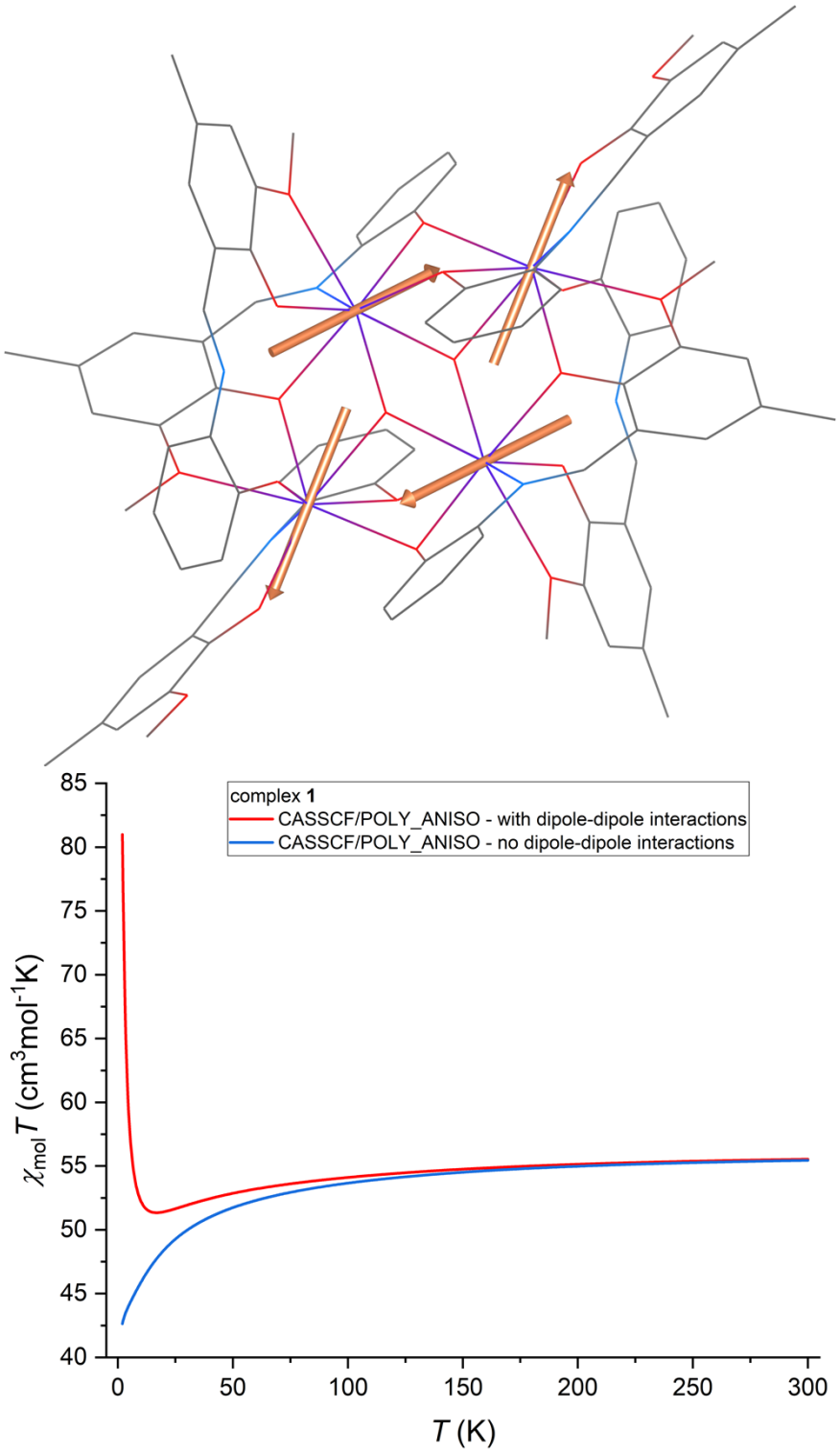

Fig. S16 The molecular structure of **1** derived from the experimental X-ray geometry used for CASSCF calculations overlaid with of g_z-tensor of the first Kramers doublet (orange arrows) (top). The calculated magnetic data for **1** using POLY_ANISO program based on respective CASSCF calculations with/without dipole-dipole interactions (bottom).

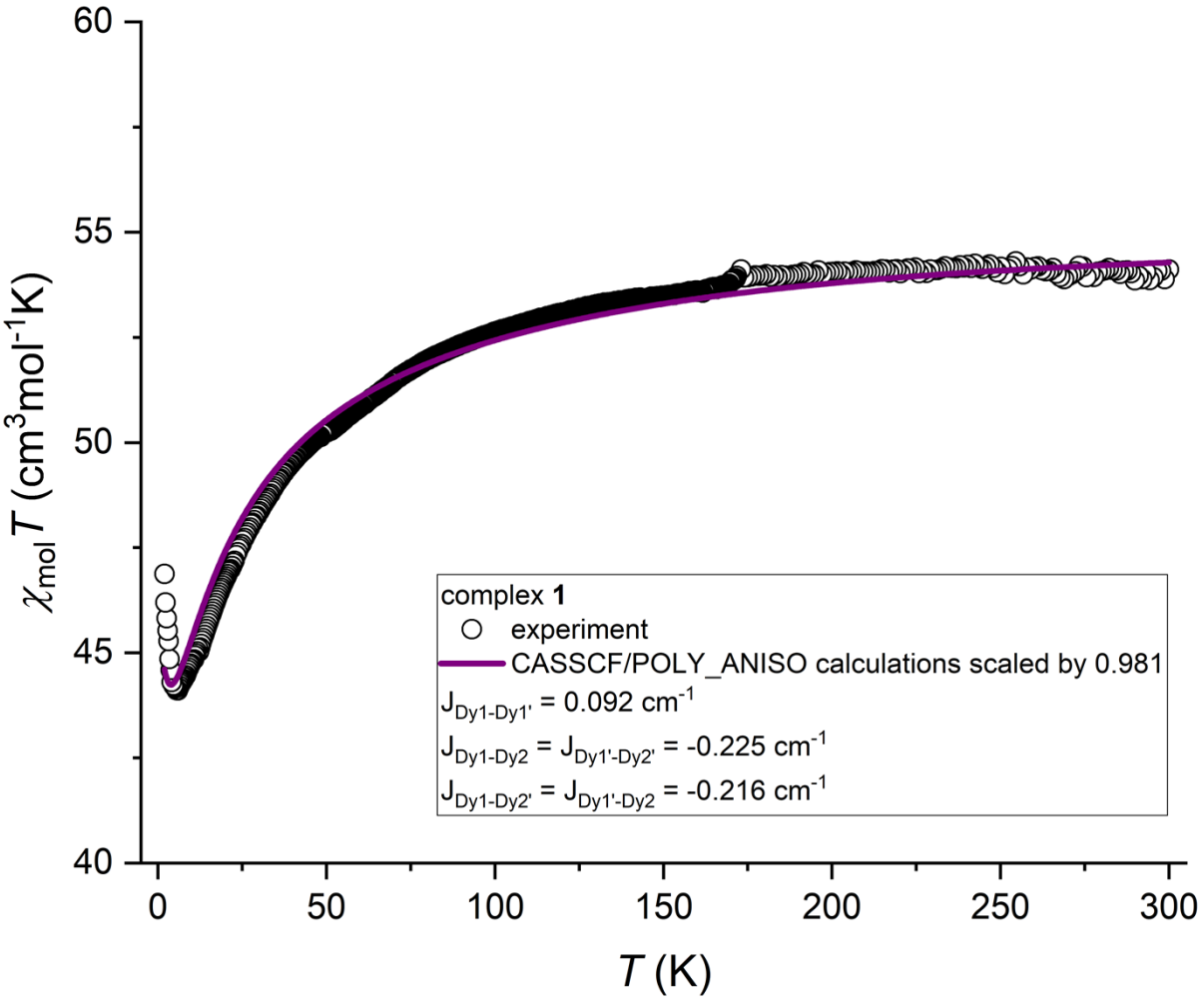

Fig. S17 The fit of experimental magnetic susceptibility of **1** utilizing CASSCF calculations, POLY_ANISO program and homemade routine.

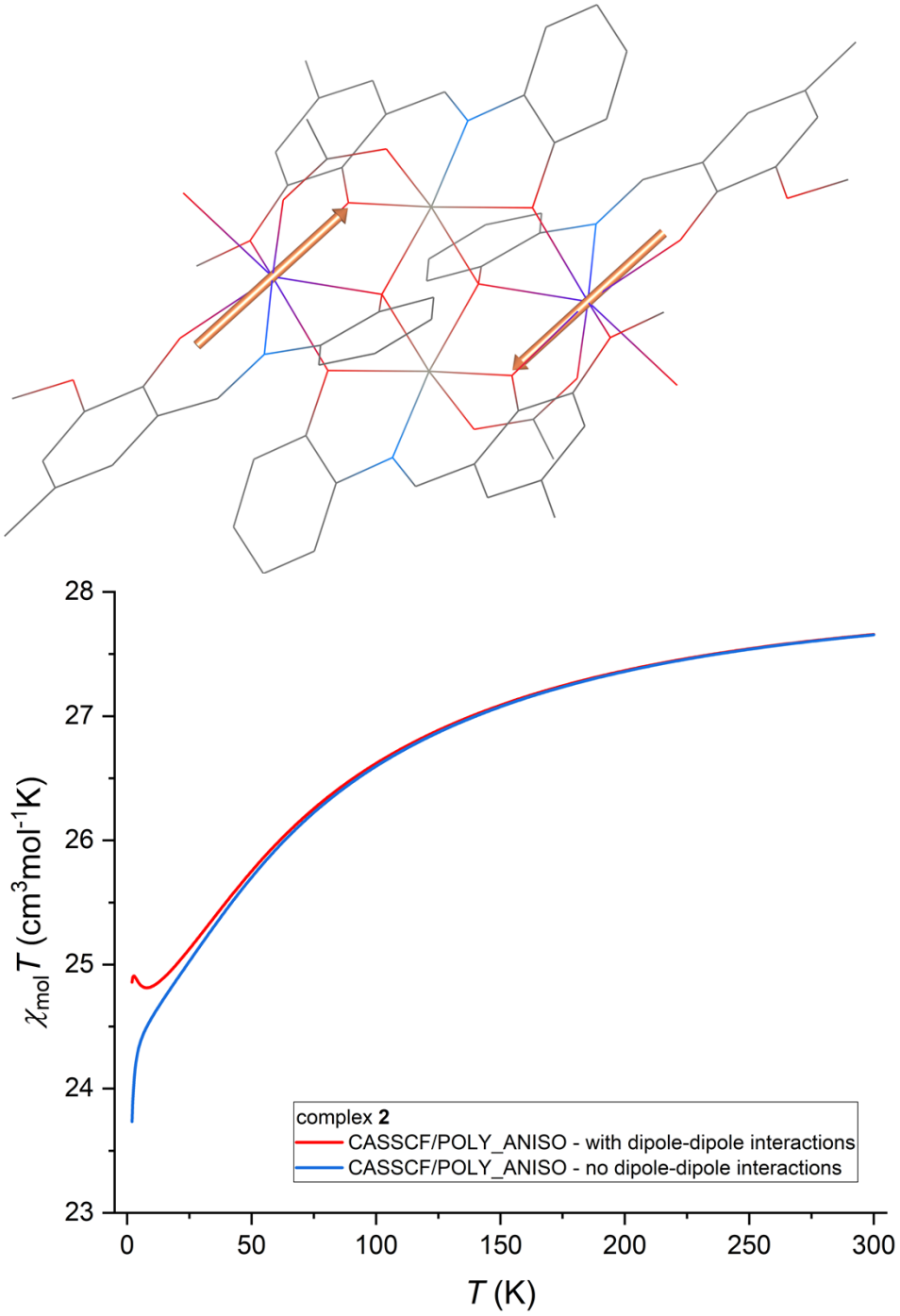

Fig. S18 The molecular structure of **2** derived from the experimental X-ray geometry used for CASSCF calculations overlaid with of g_z-tensor of the first Kramers doublet (orange arrows) (top). The calculated magnetic data for **2** using POLY_ANISO program based on respective CASSCF calculations with/without dipole-dipole interactions (bottom).

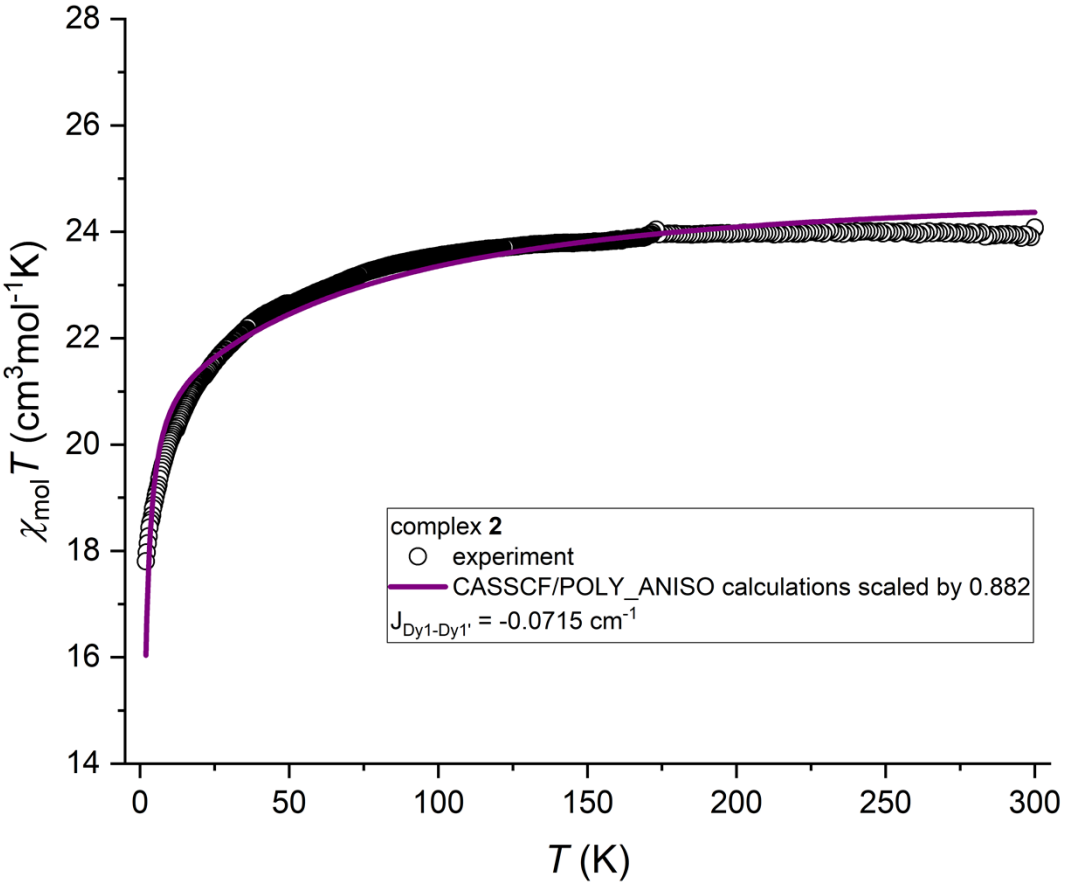

Fig. S19 The fit of experimental magnetic susceptibility of **2** utilizing CASSCF calculations, POLY_ANISO program and homemade routine.

Table S1. SHAPE analysis of the Dy(III) ion for complexes **1** and **2**.

Label	Shape	Symmetry	Distortion (**1**)		Distortion (**2**)
			Dy1	Dy2	Dy1
OP-8	Octagon	D_{8h}	33.833	31.416	31.780
HPY-8	Heptagonal pyramid	C_{7v}	20.882	20.611	23.065
HBPY-8	Hexagonal bipyramid	D_{6h}	15.042	16.144	14.437
CU-8	Cube	O_h	11.833	10.695	9.743
SAPR-8	Square antiprism	D_{4d}	4.044	**1.325**	2.455
TDD-8	Triangular dodecahedron	D_{2d}	**1.924**	2.563	**1.260**
JGBF-8	Johnson gyrobifastigium J26	D_{2d}	14.246	15.534	13.424
JETBPY-8	Johnson elongated triangular bipyramid J14	C_{3h}	27.268	25.593	26.737
JBTPR-8	Biaugmented trigonal prism J50	C_{2v}	2.493	2.338	2.054
BTPR-8	Biaugmented trigonal prism	C_{2v}	**1.503**	2.086	**1.653**
JSD-8	Snub diphenoid J84	D_{2d}	4.263	4.332	3.875
TT-8	Triakis tetrahedron	T_d	12.538	11.509	10.443
ETBPY-8	Elongated trigonal bipyramid	D_{3h}	22.768	22.995	24.472

Table S2. The splitting of the lowest multiplets for Dy1 in compound **1** calculated by CASSCF/SINGLE_ANISO together with g-values for each Kramers doublets

E (cm^{-1})	g_x	g_y	g_z
0	0.292	0.604	17.258
32	0.274	0.540	15.956
65	1.263	1.864	15.105
122	1.004	4.559	9.454
205	0.629	4.421	8.507
271	2.572	5.838	11.303
394	0.177	0.315	17.094
473	0.036	0.093	18.553

Table S3. The splitting of the lowest multiplets for Dy2 in compound **1** calculated by CASSCF/SINGLE_ANISO together with g-values for each Kramers doublets

E (cm^{-1})	g_x	g_y	g_z
0	0.094	0.205	19.538
118	1.273	3.138	15.315
174	0.991	3.264	11.639
285	3.326	6.185	9.312
353	1.433	4.285	11.673
412	0.794	1.921	16.577
463	0.937	2.166	13.915
502	0.442	1.896	17.061

Table S4. The splitting of the lowest multiplets for Dy1 in compound **2** calculated by CASSCF/SINGLE_ANISO together with g-values for each Kramers doublets

E (cm^{-1})	g_x	g_y	g_z
0	0.004	0.004	19.719
174	0.065	0.085	16.869
311	1.550	2.224	14.126
384	1.259	4.610	10.393
475	2.930	5.866	9.504
515	1.012	1.485	16.597
585	0.752	1.162	16.088
660	0.173	0.415	18.611